

Stochastic modeling of the short-time variation of cosmic rays

A. Wawrzynczak¹, R. Modzelewska², A. Gil²,

¹Institute of Computer Sciences, Siedlce University, Poland

²Institute of Mathematics and Physics, Siedlce University, Poland.

25th European Cosmic Ray Symposium
4-9 September 2016, Torino

- Parker's transport equation (PTE)
- Stochastic approach
- Fokker- Planck equation and corresponding set of stochastic differential equations (SDE)
- Numerical methods for solving SDEs
- Simulation results
- Model of the Forbush decrease of cosmic rays intensity

Parker's transport equation (1965)

$$\frac{\partial f}{\partial t} = \vec{\nabla} \cdot (K_{ij}^S \cdot \vec{\nabla} f) - (\vec{v}_d + \vec{U}) \cdot \vec{\nabla} f + \frac{R}{3} (\vec{\nabla} \cdot \vec{U}) \frac{\partial f}{\partial R}.$$

- $f \equiv f(\vec{r}, R, t)$ omnidirectional distribution function of cosmic rays in 3D space $\vec{r} \equiv (r, \theta, \varphi)$, magnetic rigidity R i time t ;
- \vec{U} - solar wind velocity,
- \vec{v}_d - drift velocity,
- K_{ij}^S - symmetric part of diffusion tensor of cosmic rays,
- $\vec{\nabla} \cdot (K_{ij}^S \cdot \vec{\nabla} f)$ - diffusion of cosmic rays,
- $(\vec{v}_d + \vec{U}) \cdot \vec{\nabla} f$ - convection due to solar wind and drift in heliospheric magnetic field,
- $\frac{R}{3} (\vec{\nabla} \cdot \vec{U}) \frac{\partial f}{\partial R}$ - energy changes of cosmic rays connected with divergence of solar wind.

Stochastic approach to the Parker's transport equation

- Is based on the assumption that any random process is independent of the other processes and single GCR particle moves in a random way, that could be described as a Brownian motion,
- The individual particle trajectory is described as a Markov stochastic process, and the system evolves probabilistically, the particle coordinates and energy are a random variables,
- First attempts:
 - Jokipii i Owens, 1975 solved 1D equation assuming no drift and constant diffusion coefficient,
 - Zhang, 1999 proposed to bring Parker transport equation to the form of the Fokker-Planck equation and define the corresponding set of stochastic differential equations of the first order including the stochastic term and by this way estimate the probabilistic trajectory of the GCR particle,
 - Gervasi et. al., 1999 presented a 1D spherically- symmetric model of the GCR transport in the heliosphere applying the stochastic Monte Carlo simulation to solve the Fokker-Planck equation.
- Recently e.g.: Strauss et. al., 2011; Kopp et. al., 2012, 2014; Bobik et. al., 2012, 2016.

time-forward

$$\frac{\partial F}{\partial t} = - \sum_i \frac{\partial (A_i \cdot F)}{\partial x_i} + \frac{1}{2} \sum_{i,j} \frac{\partial^2 (B_{ij} B_{ij}^T \cdot F)}{\partial x_i \partial x_j}.$$

time-backward

$$\frac{\partial F}{\partial t} = \sum_i A_i \frac{\partial F}{\partial x_i} + \frac{1}{2} \sum_{i,j} B_{ij} B_{ij}^T \frac{\partial^2 F}{\partial x_i \partial x_j}.$$

Corresponding stochastic Ito differential equation

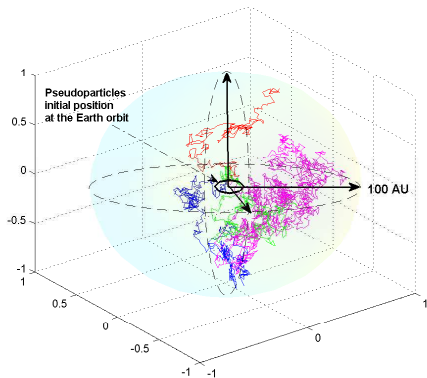
$$d\vec{r} = \vec{A}_i \cdot dt + B_{ij} \cdot d\vec{W}_i$$

- $d\vec{r}$ - the individual pseudoparticle trajectory in the phase space
- $d\vec{W}_i$ the Wiener process, commonly written as $dW_i = \sqrt{dt} \cdot dw_i$, where dw_i is the randomly fluctuating term with Gaussian distribution.

time-forward vs. time-backward integration

time-forward integration

- pseudoparticles are initialized from diverse boundary points, being for the GCR particles the entrance to the heliosphere. After that, their trajectories are traced up to the target position, e.g. Earth orbit at 1 astronomical unit (AU),
- a high number of pseudoparticles has to be initialized to obtain a robust statistic, because plenty of them do not reach the target position,
- time consuming.

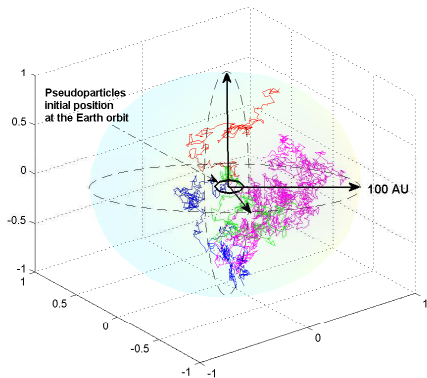


The sample pseudoparticles trajectories within the heliosphere.

time-forward vs. time-backward integration

time-backward integration

- Pseudoparticles are initialized from point of interest (e.g. Earth orbit) and are traced backward in time until crossing the heliospheric boundary (in this paper this boundary is assumed at 100 AU),
- advantage - the number of 'useless' particles is reduced.
- time-backward integration is much more efficient in the case of cosmic ray propagation in the heliosphere.



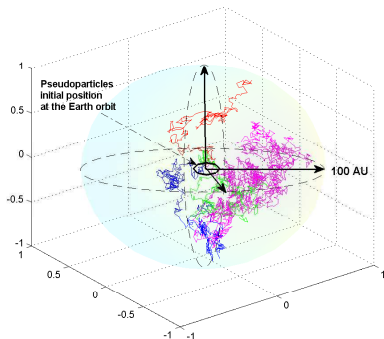
The sample pseudoparticles trajectories within the heliosphere.

Value of distribution function $f(\vec{r}, R)$

- the value of the particle distribution function, $f(\vec{r}, R)$, for the starting point can be found as an average value of $f_{LIS}(R)$ for pseudoparticles characteristics at the entry positions

$$f(\vec{r}, R) = \frac{1}{N} \sum_{n=1}^N f_{LIS}(R),$$

- where $f_{LIS}(R)$ is the cosmic ray local interstellar spectrum (LIS) for rigidity R of the n^{th} particle at the exit/entrance point.
- We considered the various forms of LIS (Burger et al., 2000; Webber and Lockwood, 2001; Potgieter et. al., 2014, Vos and Potgieter, 2015) and obtained comparable results.



The sample pseudoparticles trajectories within the heliosphere.

The Parker equation as the time-backward FPE diffusion equation

$$\begin{aligned}\frac{\partial f}{\partial t} = & a_1 \frac{\partial^2 f}{\partial r^2} + a_2 \frac{\partial^2 f}{\partial \theta^2} + a_3 \frac{\partial^2 f}{\partial \varphi^2} + a_4 \frac{\partial^2 f}{\partial r \partial \theta} + a_5 \frac{\partial^2 f}{\partial r \partial \varphi} + \\ & + a_6 \frac{\partial^2 f}{\partial \theta \partial \varphi} + a_7 \frac{\partial f}{\partial r} + a_8 \frac{\partial f}{\partial \theta} + a_9 \frac{\partial f}{\partial \varphi} + a_{10} \frac{\partial f}{\partial R}.\end{aligned}$$

Set of SDEs for Parker's transport equation

$$\begin{aligned}dr &= a_7 \cdot dt + [B \cdot dW]_r \\ d\theta &= a_8 \cdot dt + [B \cdot dW]_\theta \\ d\varphi &= a_9 \cdot dt + [B \cdot dW]_\varphi \\ dR &= a_{10} \cdot dt.\end{aligned}$$

Set of SDEs for Parker's transport equation

$$\begin{aligned}dr &= a_7 \cdot dt + [B \cdot dW]_r \\d\theta &= a_8 \cdot dt + [B \cdot dW]_\theta \\d\varphi &= a_9 \cdot dt + [B \cdot dW]_\varphi \\dR &= a_{10} \cdot dt.\end{aligned}$$

$$B_{i,j} = \begin{bmatrix} \sqrt{2a_1} & 0 & 0 \\ \frac{a_4}{\sqrt{2a_1}} & \sqrt{2a_2 - \frac{a_4^2}{2a_1}} & 0 \\ \frac{a_5}{\sqrt{2a_1}} & \frac{a_6 - \frac{a_4 a_5}{2a_1}}{B_{\theta\theta}} & \sqrt{2a_3 - B_{\varphi r}^2 - B_{\varphi\theta}^2} \end{bmatrix}.$$

Equation coefficients

$$a_1 = K_{rr}^S, a_2 = \frac{K_{\theta\theta}^S}{r^2}, a_3 = \frac{K_{\varphi\varphi}^S}{r^2 \sin^2\theta}, a_4 = \frac{2K_{r\theta}^S}{r},$$

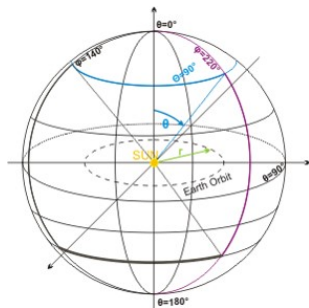
$$a_5 = \frac{2K_{r\varphi}^S}{r \sin\theta}, a_6 = \frac{2K_{\theta\varphi}^S}{r^2 \sin\theta}$$

$$a_7 = \frac{2}{r} K_{rr}^S + \frac{\partial K_{rr}^S}{\partial r} + \frac{\text{ctg}\theta}{r} K_{\theta r}^S + \frac{1}{r} \frac{\partial K_{\theta r}^S}{\partial \theta} + \frac{1}{r \sin\theta} \frac{\partial K_{\varphi r}^S}{\partial \varphi} - U - v_{d,r}$$

$$a_8 = \frac{K_{r\theta}^S}{r^2} + \frac{1}{r} \frac{\partial K_{r\theta}^S}{\partial r} + \frac{1}{r^2} \frac{\partial K_{\theta\theta}^S}{\partial \theta} + \frac{\text{ctg}\theta}{r^2} K_{\theta\theta}^S + \frac{1}{r^2 \sin\theta} \frac{\partial K_{\varphi\theta}^S}{\partial \varphi} - \frac{1}{r} v_{d,\theta}$$

$$a_9 = \frac{K_{r\varphi}^S}{r^2 \sin\theta} + \frac{1}{r \sin\theta} \frac{\partial K_{r\varphi}^S}{\partial r} + \frac{1}{r^2 \sin\theta} \frac{\partial K_{\theta\varphi}^S}{\partial \theta} + \frac{1}{r^2 \sin^2\theta} \frac{\partial K_{\varphi\varphi}^S}{\partial \varphi} - \frac{1}{r \sin\theta} v_{d,\varphi}$$

$$a_{10} = \frac{R}{3} \nabla \cdot U.$$



Equation coefficients

- $K_{ij} = K_{ij}^{(S)} + K_{ij}^{(A)}$ 3D anisotropic diffusion tensor containing symmetric $K_{ij}^{(S)}$ and antisymmetric $K_{ij}^{(A)}$ part (Alania 1978, 2002)

-

$$K_{ij} = K_{\parallel} \begin{pmatrix} \cos\delta^2 \cos\psi^2 + \beta(\cos\delta^2 \sin\psi^2 + \sin\delta^2) & \sin\delta \cos\delta \cos\psi^2(1-\beta) & \sin\psi \cos\delta \cos\psi(\beta-1) \\ \sin\delta \cos\delta \cos^2\psi(1-\beta) & \sin^2\delta \cos^2\psi + \beta(\sin^2\delta \sin^2\psi + \cos^2\delta) & \sin\delta \sin\psi \cos\psi(\beta-1) \\ \cos\delta \sin\psi \cos\psi(\beta-1) & \sin\delta \sin\psi \cos\psi(\beta-1) & \sin^2\psi + \beta \cos^2\psi \end{pmatrix} +$$

$$+ K_{\perp} \begin{pmatrix} 0 & \mp \beta_1 \sin\psi & \mp \beta_1 \sin\delta \cos\psi \\ \pm \beta_1 \sin\psi & 0 & \pm \beta_1 \cos\delta \cos\psi \\ \pm \beta_1 \sin\delta \cos\psi & \mp \beta_1 \cos\delta \cos\psi & 0 \end{pmatrix}$$

- drift velocity $v_{d,i} = \frac{\partial K_{ij}^{(A)}}{\partial x_j}$ (Jokipi, 1977)
- $\psi = \text{arctg} \frac{-B_{\varphi}}{B_r} = \text{arctg} \frac{\Omega r \sin\theta}{U}$
- $\delta = \text{arctg} \frac{-B_{\theta}}{B_r}$
- $\beta = \frac{K_{\perp}}{K_{\parallel}}$
- $\beta_1 = \frac{K_d}{K_{\parallel}}$

Euler- Maruyama method-basic numerical approximation of the SDE solution

$$dX_t = f(X_t)dt + g(X_t)dW_t \quad X_{j+1} = X_j + f \cdot dt + g \cdot dW_t$$

depending on the level of the Ito - Taylor expansion, the order of convergence γ increases: the Euler- Maruyama method $\gamma = 0.5$, Milstein method $\gamma = 1$ and Stochastic Runge - Kutta- $\gamma = 1.5$)

$$X_{j+1} = \underbrace{X_j + f \cdot dt + g \cdot dW_t}_{\text{Euler - Murayama}} + \underbrace{\frac{1}{2}g \cdot g'(dW_j^2 - dt)}_{\text{Milstein}} + \Phi$$

$\underbrace{\hspace{15em}}_{\text{Stochastic Runge-Kutta}}$

Higher order approximation to the numerical solution of SDEs

$$X_{j+1} = \underbrace{X_j + f \cdot dt + g \cdot dW_t}_{\text{Euler-Murayama}} + \frac{1}{2} g \cdot g' (dW_j^2 - dt) + \Phi$$
$$\underbrace{\hspace{10em}}_{\text{Milstein}}$$
$$\underbrace{\hspace{15em}}_{\text{Stochastic Runge-Kutta}}$$

$$\begin{aligned} \Phi = & f' \cdot g \cdot dZ_j + \frac{1}{2} (f \cdot f' + \frac{1}{2} g^2 \cdot f'') dt^2 + \\ & + (f \cdot g' + \frac{1}{2} g^2 \cdot g'') (dW_j \cdot dt - dZ_j) + \\ & + \frac{1}{2} g (g \cdot g'' + g'^2) (\frac{1}{3} dW_j^2 - dt) dW_j \end{aligned}$$

Euler-Murayama method for the numerical approximation of the SDEs solution

$$\begin{aligned}r_{i+1} &= r_i + dr_{EM} \\ \theta_{i+1} &= \theta_i + d\theta_{EM} \\ \varphi_{i+1} &= \varphi_i + d\varphi_{EM} \\ R_{i+1} &= R_i + dR_{EM}\end{aligned}\tag{1}$$

where

$$\begin{aligned}dr_{EM} &= a_7 \cdot dt + B_{rr} \cdot dW_r \\ d\theta_{EM} &= a_8 \cdot dt + B_{\theta r} \cdot dW_r + B_{\theta\theta} \cdot dW_\theta \\ d\varphi_{EM} &= a_9 \cdot dt + B_{\varphi r} \cdot dW_r + B_{\varphi\theta} \cdot dW_\theta + B_{\varphi\varphi} \cdot dW_\varphi \\ dR_{EM} &= a_{10} \cdot dt\end{aligned}\tag{2}$$

for the higher order methods we have (dr):

$$dr = \underbrace{a_r \cdot dt + B_{rr} \cdot dW_r}_{\text{Euler-Murayama}} + \underbrace{\frac{1}{2} B_{rr} \frac{\partial B_{rr}}{\partial r} (dW_r^2 - dt) + \frac{1}{2} B_{rr} \frac{\partial B_{rr}}{\partial r} (dW_r^2 - dt)}_{\text{Milstein}} + \Phi_1$$

$\underbrace{\hspace{15em}}_{\text{Stochastic Runge-Kutta}}$

$$\begin{aligned} \Phi_1 = & B_{rr} \cdot dZ_r \frac{\partial a_r}{\partial r} + \frac{1}{2} (a_r \frac{\partial a_r}{\partial r} + \frac{1}{2} B_{rr}^2 \frac{\partial^2 a_r}{\partial r^2}) dt^2 + \\ & + (a_r \frac{\partial B_{rr}}{\partial r} + \frac{1}{2} B_{rr}^2 \frac{\partial^2 B_{rr}}{\partial r^2}) (dW_r dt - dZ_r) \\ & + \frac{1}{2} B_{rr} (B_{rr} \frac{\partial^2 B_{rr}}{\partial r^2} + (\frac{\partial B_{rr}}{\partial r})^2) (\frac{1}{3} dW_r^2 - dt) dW_r \end{aligned}$$

for the higher order methods we have $(d\theta)$:

$$\begin{aligned}
 d\theta &= \underbrace{a_{\theta} \cdot dt + B_{\theta r} \cdot dW_r + B_{\theta\theta} \cdot dW_{\theta}}_{\text{Euler-Maruyama}} + \frac{1}{2} B_{\theta r} \frac{\partial B_{\theta r}}{\partial \theta} (dW_r^2 - dt) + \frac{1}{2} B_{\theta\theta} \frac{\partial B_{\theta\theta}}{\partial \theta} (dW_{\theta}^2 - dt) + \Phi_2 \\
 &\underbrace{\hspace{15em}}_{\text{Milstein}} \\
 &\underbrace{\hspace{15em}}_{\text{stochastic Runge-Kutta}}
 \end{aligned} \tag{3}$$

$$\begin{aligned}
 \Phi_2 &= B_{\theta r} \cdot dZ_r \frac{\partial a_{\theta}}{\partial \theta} + \frac{1}{2} \left(a_{\theta} \frac{\partial a_{\theta}}{\partial \theta} + \frac{1}{2} B_{\theta r}^2 \frac{\partial^2 a_{\theta}}{\partial \theta^2} \right) dt^2 + \\
 &+ \left(a_{\theta} \frac{\partial B_{\theta r}}{\partial \theta} + \frac{1}{2} B_{\theta r}^2 \frac{\partial^2 B_{\theta r}}{\partial \theta^2} \right) (dW_r \cdot dt - dZ_r) + \\
 &+ \frac{1}{2} B_{\theta r} \left(B_{\theta r} \frac{\partial^2 B_{\theta r}}{\partial \theta^2} + \left(\frac{\partial B_{\theta r}}{\partial \theta} \right)^2 \right) \left(\frac{1}{3} dW_r^2 - dt \right) dW_r + \\
 &+ B_{\theta\theta} \cdot dZ_{\theta} \frac{\partial a_{\theta}}{\partial \theta} + \frac{1}{2} \left(a_{\theta} \frac{\partial a_{\theta}}{\partial \theta} + \frac{1}{2} B_{\theta\theta}^2 \frac{\partial^2 a_{\theta}}{\partial \theta^2} \right) dt^2 + \\
 &+ \left(a_{\theta} \frac{\partial B_{\theta\theta}}{\partial \theta} + \frac{1}{2} B_{\theta\theta}^2 \frac{\partial^2 B_{\theta\theta}}{\partial \theta^2} \right) (dW_{\theta} \cdot dt - dZ_{\theta}) + \\
 &+ \frac{1}{2} B_{\theta\theta} \left(B_{\theta\theta} \frac{\partial^2 B_{\theta\theta}}{\partial \theta^2} + \left(\frac{\partial B_{\theta\theta}}{\partial \theta} \right)^2 \right) \left(\frac{1}{3} dW_{\theta}^2 - dt \right) dW_{\theta}
 \end{aligned}$$

for the higher order methods we have $(d\varphi)$:

$$d\varphi = \underbrace{a_{\varphi} \cdot dt + B_{\varphi r} \cdot dW_r + B_{\varphi\theta} \cdot dW_{\theta} + B_{\varphi\varphi} \cdot dW_{\varphi}}_{\text{Euler-Maruyama}} + \Phi_3 + \Phi_4$$

$$\underbrace{\hspace{10em}}_{\text{Milstein}}$$

$$\underbrace{\hspace{15em}}_{\text{stochastic Runge-Kutta}}$$

$$dR = a_{10} \cdot dt.$$

$$\Phi_3 = \frac{1}{2} B_{\varphi r} \frac{\partial B_{\varphi r}}{\partial \varphi} (dW_r^2 - dt) + \frac{1}{2} B_{\varphi\theta} \frac{\partial B_{\varphi\theta}}{\partial \varphi} (dW_{\theta}^2 - dt) + \frac{1}{2} B_{\varphi\varphi} \frac{\partial B_{\varphi\varphi}}{\partial \varphi} (dW_{\varphi}^2 - dt);$$

$$\Phi_4 = B_{\varphi r} \cdot dZ_r \frac{\partial a_{\varphi}}{\partial \varphi} + \frac{1}{2} (a_{\varphi} \frac{\partial a_{\varphi}}{\partial \varphi} + \frac{1}{2} B_{\varphi r}^2 \frac{\partial^2 a_{\varphi}}{\partial \varphi^2}) dt^2 + (a_{\varphi} \frac{\partial B_{\varphi r}}{\partial \varphi} + \frac{1}{2} B_{\varphi r}^2 \frac{\partial^2 B_{\varphi r}}{\partial \varphi^2}) (dW_r \cdot dt - dZ_r) + \frac{1}{2} B_{\varphi r} (B_{\varphi r} \frac{\partial^2 B_{\varphi r}}{\partial \varphi^2} + (\frac{\partial B_{\varphi r}}{\partial \varphi})^2) (\frac{1}{3} dW_r^2 - dt) dW_r + B_{\varphi\theta} \cdot dZ_{\theta} \frac{\partial a_{\varphi}}{\partial \varphi} + \frac{1}{2} (a_{\varphi} \frac{\partial a_{\varphi}}{\partial \varphi} + \frac{1}{2} B_{\varphi\theta}^2 \frac{\partial^2 a_{\varphi}}{\partial \varphi^2}) dt^2 + (a_{\varphi} \frac{\partial B_{\varphi\theta}}{\partial \varphi} + \frac{1}{2} B_{\varphi\theta}^2 \frac{\partial^2 B_{\varphi\theta}}{\partial \varphi^2}) (dW_{\theta} \cdot dt - dZ_{\theta}) + \frac{1}{2} B_{\varphi\theta} (B_{\varphi\theta} \frac{\partial^2 B_{\varphi\theta}}{\partial \varphi^2} + (\frac{\partial B_{\varphi\theta}}{\partial \varphi})^2) (\frac{1}{3} dW_{\theta}^2 - dt) dW_{\theta} + B_{\varphi\varphi} \cdot dZ_{\varphi} \frac{\partial a_{\varphi}}{\partial \varphi} + \frac{1}{2} (a_{\varphi} \frac{\partial a_{\varphi}}{\partial \varphi} + \frac{1}{2} B_{\varphi\varphi}^2 \frac{\partial^2 a_{\varphi}}{\partial \varphi^2}) dt^2 + (a_{\varphi} \frac{\partial B_{\varphi\varphi}}{\partial \varphi} + \frac{1}{2} B_{\varphi\varphi}^2 \frac{\partial^2 B_{\varphi\varphi}}{\partial \varphi^2}) (dW_{\varphi} \cdot dt - dZ_{\varphi}) + \frac{1}{2} B_{\varphi\varphi} (B_{\varphi\varphi} \frac{\partial^2 B_{\varphi\varphi}}{\partial \varphi^2} + (\frac{\partial B_{\varphi\varphi}}{\partial \varphi})^2) (\frac{1}{3} dW_{\varphi}^2 - dt) dW_{\varphi}.$$

- initial condition-empty heliosphere
 $f_i(0.01AU < r < 100AU, \theta, \varphi, R, 0) = 0$, (Pei et. al., 2010)
- inner reflecting radial boundary
 $\frac{\partial f}{\partial r} = 0$ at $r = 0.001$ AU,
- boundary conditions (as in Kopp et. al., 2012)
 - $\varphi_i < 0 \rightarrow \varphi_i = \varphi_i + 2\pi$;
 - $\varphi_i > 2\pi \rightarrow \varphi_i = \varphi_i - 2\pi$;
 - $\theta_i < 0 \rightarrow \theta_i = -\theta_i$ & $\varphi_i = \varphi_i \pm \pi$
 - $\theta_i > \pi \rightarrow \theta_i = 2\pi - \theta_i$ & $\varphi_i = \varphi_i \pm \pi$

Results

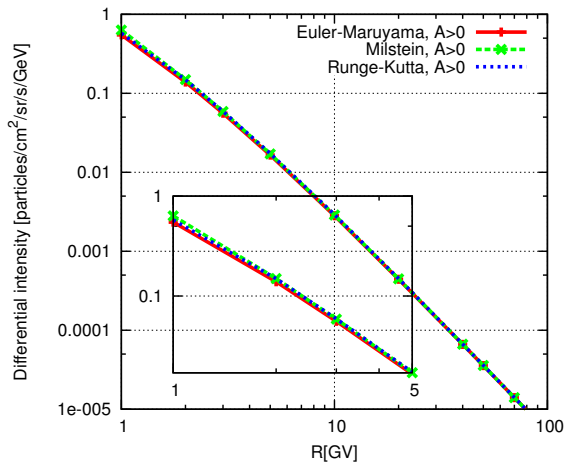


Figure Simulated galactic protons rigidity spectra for the pseudoparticles initialized from position $r = 1AU$, $\theta = 90^\circ$, $\varphi = 180^\circ$ for the $A > 0$ obtained by applying the Euler-Maruyama, Milstein and stochastic Runge-Kutta methods.

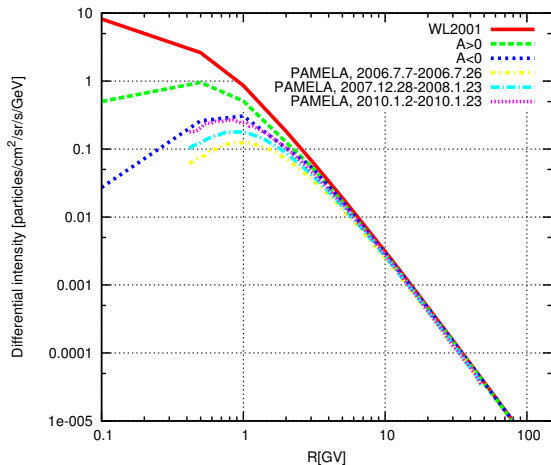


Figure Simulated galactic protons rigidity spectra for the $A > 0$ and $A < 0$ in comparison with spectra reported by PAMELA (Adriani et. al., 2013).

Results

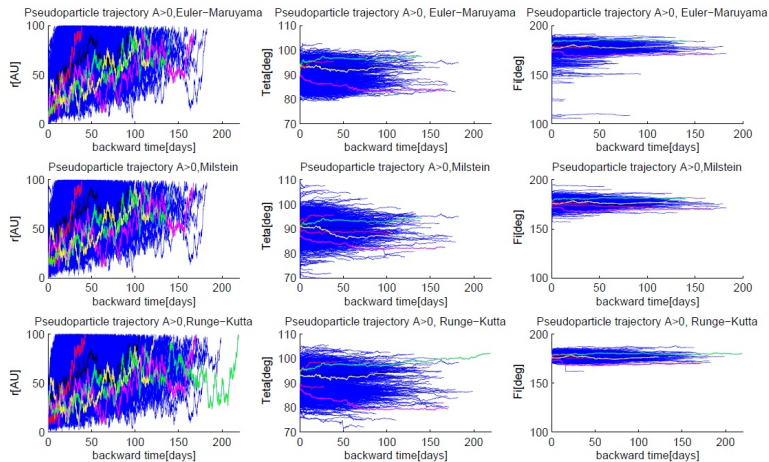


Figure Trajectories of the pseudoparticles with rigidity of 10 GV for the $A > 0$ obtained by applying the Euler-Maruyama, Milstein and stochastic Runge- Kutta methods. The specific colors highlight the trajectories of the sample pseudoparticles, based on the same Wiener process, traced backward in time from the heliosphere boundary until they reach the position of Earth.

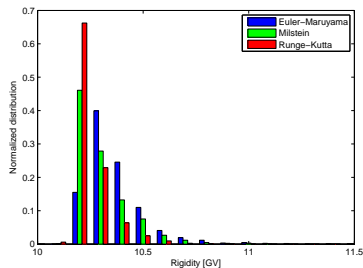


Figure The histograms of the particles rigidity for the pseudoparticles initialized with rigidity 10 GV from position $r = 1AU$, $\theta = 90^\circ$, $\varphi = 180^\circ$ for the $A > 0$.

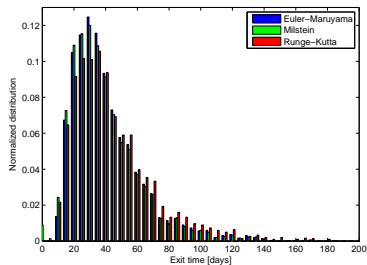


Figure The histograms of the particles exit time for the pseudoparticles initialized with rigidity 10 GV from position $r = 1AU$, $\theta = 90^\circ$, $\varphi = 180^\circ$ for the $A > 0$.

Results

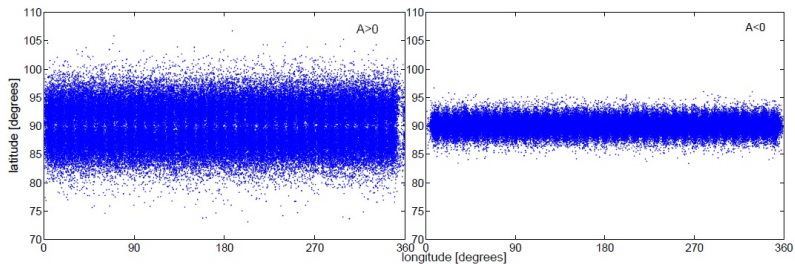
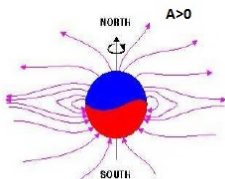
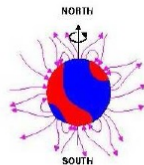


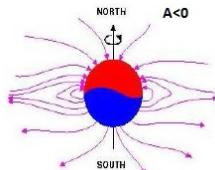
Figure Latitude vs. longitude distribution of simulated pseudoparticles (protons) for the $A > 0$ and $A < 0$ solar magnetic cycle.



CORONAL MAGNETIC FIELD LINES AT SOLAR MINIMUM ACTIVITY



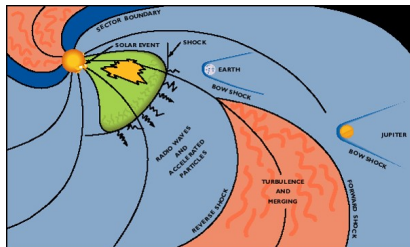
CORONAL MAGNETIC FIELD LINES AT SOLAR MAXIMUM ACTIVITY



CORONAL MAGNETIC FIELD LINES AT NEXT SOLAR MINIMUM

Model of the Forbush decrease

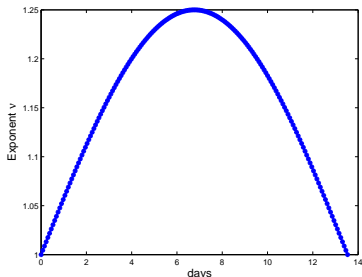
- The Forbush decrease (Fd) is called the decrease of the GCR intensity registered at Earth. This decrease is connected with the strengthen of the Interplanetary Magnetic Field (IMF) and other parameters in connection with the solar flares or coronal mass ejecta. (Forbush, 1937).



- We assume that during Fd the disturbances in the interplanetary space cause near the Earth's orbit the gradual decrease of the diffusion coefficient as the effect of the increase in the IMF turbulence.
- We simulate this process by gradual decrease and then gradual increase of the diffusion coefficient vs. heliolongitude.
- The diffusion coefficient K_{\parallel} of GCR particles has a form:
 $K_{\parallel} = K_0 \cdot K(r) \cdot K(R, \nu)$, where $K_0 = 10^{21} \text{ cm}^2/\text{s}$,
 $K(r) = 1 + 0.5 \cdot (r/1\text{AU})$.
- $K(R, \nu) = (R/R_0)^{2-\nu}$, where $R_0 = 1\text{GV}$ according to Quasi Linear theory (Jokipii, 1966; Shalchi, 2009)

Model of the Forbush decrease

- $K(R, \nu) = (R/R_0)^{2-\nu}$, where $R_0 = 1\text{GV}$ according to Quasi Linear theory (Jokipii, 1966; Shalchi, 2009)
- ν is the exponent of the PSD of the IMF.
- The increase of the exponent ν reflects the increase of the IMF turbulence during the Fd (e.g. Wawrzynczak, Alania, 2008,2010).
- $\nu = 1 + 0.25\sin(\varphi - 90^\circ)$ for $r < 30\text{AU}$ and $90^\circ \leq \varphi \leq 270^\circ$.



Model of the Forbush decrease

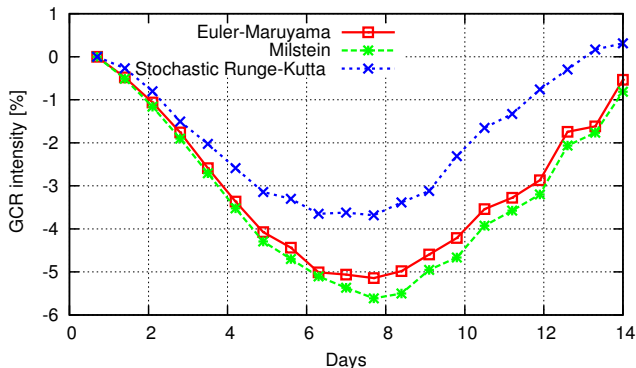


Figure Changes of the expected amplitudes of the Fd of the GCR intensity at the Earth orbit, for the rigidity of 10 GV based on the solutions of the SDEs by Euler-Maruyama, Milstein and stochastic Runge-Kutta methods.

Model of the Forbush decrease

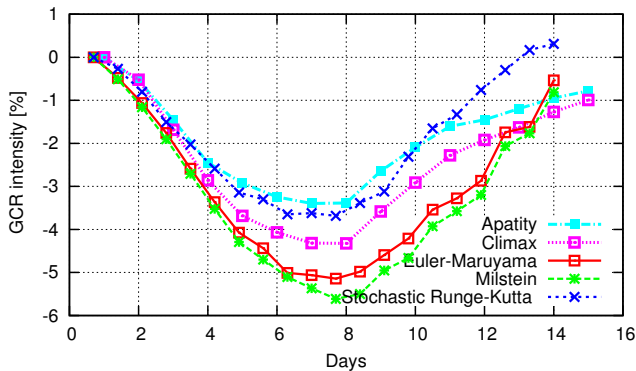


Figure Changes of the expected amplitudes of the Fd of the GCR intensity at the Earth orbit, for the rigidity of 10 GV based on the solutions of the SDEs by Euler-Maruyama, Milstein and stochastic Runge-Kutta methods in comparison with the GCR intensity registered by Apatity and Climax neutron monitors during the Fd on 16-30 Jun 2003.

Conclusions

- We presented the numerical solution of the Parker transport equation by means of a numerical solution of the set of stochastic differential equations driven by a Wiener process with the strong order Euler-Maruyama, Milstein, and stochastic Runge-Kutta methods.
- The SDEs were integrated backward in time in the heliocentric spherical coordinates applying the full 3D anisotropic diffusion tensor.
- We presented the model of the Forbush decrease of the GCR intensity obtained based on the stochastic approach to the solution of the Parker transport equation.
- We showed that application of the higher order methods (especially stochastic Runge-Kutta) significantly increased the statistical accuracy of the numerical solution in the case of the model of the short-time variations of the GCR intensity.

Thank You!

- This work is supported by The Polish National Science Centre grant **SONATA** awarded by decision number DEC-2012/07/D/ST6/02488.
- We thank the principal investigators of Apatity and Climax neutron monitors for the ability to use their data.